Synthesis of Dense Fine-Grained Ceramics by Sol–Gel Technique of RE-substituted $Bi_{1-x}A_xFeO_3$ Nanopowders (A = La^{3+}, Y^{3+}, Dy^{3+}, Ce^{3+}): Structural, Electrical, and Magnetic Characterization

D.S. GARCÍA-ZALETA, A.M. TORRES-HUERTA, and M.A. DOMÍNGUEZ-CRESPO

In this work, ceramics with the formula $Bi_{1-x}A_xFeO_3$ (A = La^{3+}, Y^{3+}, Ce^{3+} and Dy^{3+}) using concentrations up to $x = 0.20$ were prepared by the sol–gel method. The effects of the diverse cations on the phase formation, grain size, as well as the electrical and magnetic properties were studied. The XRD results displayed the rhombohedral structure in all the ceramics as well as successful formation of single-phase compounds using lanthanum cations ($x = 0.10$ to 0.15). Scanning Electron Microscopy showed a non-homogeneous microstructure, consisting of grains with irregular morphology as well as the influence of the sintering method (spark plasma and conventional sintering) on the grain densification. Electric impedance spectroscopy measurements were performed to evaluate the electric properties, thus showing a slight increase in the permittivity values. Finally, the magnetic characterization showed an interesting increment in the coercive field up to ~7782 Oe with La^{3+} cations as well as a notable dependence with the dopant.

DOI: 10.1007/s11661-016-3330-0

I. INTRODUCTION

MULTIFERROIC materials have attracted much attention due to their multifunctional properties and their potential applications for new device functions, *i.e.,* advanced spintronics devices allow to control the ferroelectricity using a magnetic field or to manipulate the magnetism using an electric field.[1] The bismuth ferrite ($BiFeO_3$ or BFO) is a representative multiferroic material which crystallizes in ABO_3-typed perovskite structure with *R3c* space group at room temperature; it exhibits some of the highest values in the family of the multiferroic materials: antiferromagnetic behavior below the Neel temperature T_N ~643 K to 653 K (370 °C to 380 °C) and ferroelectric behavior below the Curie temperature T_c ~1093 K to 1123 K (820 °C to 850 °C).[2–5] Many studies have produced BFO materials using several synthesis methods, such as sol–gel,[6] co-precipitation,[7] solid-state route,[8] microwave-hydrothermal,[9] combustion method,[10] *etc.*; however, the difficulty in preparing pure phase BFO compounds due to various competing phases that could be formed[11–13] as well as the wide difference in ferroic transition temperature precludes the potential application of this compound.[14]

In order to improve the electrical properties of BFO, many researchers have found that a partial substitution of A-site ion with rare-earth or alkaline-earth ions results in the reduction of the leakage current density.[15] In addition, the use of some cations such as Y^{3+}, Pr^{3+}, Dy^{3+}, Ce^{3+}, and La^{3+} has demonstrated worthy results;[10,16–20] nevertheless, in the majority of the studies, the secondary phases could not be avoided. On the other hand, it is known that BFO exhibits G-type antiferromagnetic ordering with a long-wavelength spiral modulation of magnetic spins which apparently prevents development of a net magnetization in this material;[21,22] but, the partial substitutions have been beneficial for the magnetic response of the BFO ceramics.[23,24]

In this report, different rare-earth elements La, Y, Dy, and Ce were chosen to substitute at Bi-site of $BiFeO_3$ using the sol–gel technique. As these elements (in 3+ valence state) have their radii smaller than Bi^{3+}, they can occupy Bi^{3+} positions, and moreover, their bond energies with O^{2-} are greater than that of Bi-O bond energy which may reduce oxygen vacancies during synthesis to obtain a single phase. It is also established the influence of Bi^{3+} substitution on the structural, electrical, and magnetic properties.

II. MATERIALS AND METHODS

A. *$Bi_{1-x}A_xFeO_3$ Synthesis*

$Bi_{1-x}A_xFeO_3$ (A = La^{3+}, Y^{3+}, Ce^{3+}, Dy^{3+}, $x = 0$ to 0.20) compounds were synthesized using the sol–gel

D.S. GARCÍA-ZALETA, Professor, is with Universidad Juárez Autónoma de Tabasco, DAMJ, Tabasco, Mexico, and also with the Programa de Doctorado en Tecnología Avanzada, CICATA-Altamira, Grupo CIAMS, Instituto Politécnico Nacional, Km 14.5, Carretera Tampico-Puerto Industrial Altamira, C. P. 89600, Altamira, Tamps, Mexico. A.M. TORRES-HUERTA and M.A. DOMÍNGUEZ-CRESPO, Professors and Researchers, are with the CICATA-Altamira, Grupo CIAMS, Instituto Politécnico Nacional. Contact e-mail: atohuer@hotmail.com
Manuscript submitted June 24, 2015.
Article published online January 21, 2016

method. The starting materials were bismuth nitrate ($Bi(NO_3)_3{\cdot}5H_2O$) (Sigma-Aldrich, 98.0 pct), iron nitrate ($Fe(NO_3)_3\ 9H_2O$) (Sigma-Aldrich, 98.0 pct), lanthanum nitrate ($La(NO_3)_3{\cdot}6H_2O$), yttrium nitrate ($Y(NO_3)_3\ 6H_2O$), cerium nitrate ($Ce(NO_3)_3{\cdot}6H_2O$), and dysprosium nitrate ($Dy(NO_3)_3\ 3H_2O$) (Sigma-Aldrich, 99.9 pct). Due to the stoichiometric of $BiFeO_3$, proper amounts of the different precursors were mixed with acetic acid (CH_3COOH) (Sigma-Aldrich, 99.7 pct), and methoxyethanol ($CH_3OCH_2CH_2OH$) (Sigma-Aldrich, 99.8 pct); in order to obtain a homogeneous solution, it was stirred up to precursors were dissolved. Later, the solution was gradually evaporated between 323 K and 343 K (50 °C and 70 °C) during 320 to 820 minutes. After, a milling process was used to homogenize the powders. Finally, the powders received an optimal thermal treatment at 873 K (600 °C) for 60 minutes followed of a quenching process to complete the procedure. A general scheme of the process is shown in Figure 1.

In order to densify the powders, conventional sintering and spark plasma technique were carried out. On conventional sintering, the powders were pressed at 620 MPa to get disk-shaped samples of 11 mm of diameter and a thickness of 1 mm before being sintered in a conventional furnace at 1073 K (800 °C) during 60 minutes. On the second method, the powders were pre-loaded into a graphite-die set, axially pressed at 70 MPa and thermally treated at 1073 K (800 °C) in a commercial spark plasma sintering device (Sumitomo, Dr. Sinter 1050).

B. *Sample Characterization*

The obtained powders and sintered pellets were characterized by X-ray diffraction technique (XRD) using an X-ray diffractometer (Bruker D8 advanced), using Cu Kα radiation ($\lambda = 1.054$ Å) at 35 kV and 25 mA. The data were collected at room temperature in the 2θ range from 20 to 100 deg with a step size of 0.017 deg and a step time of 3 seconds using a Lynxeye detector. The crystal structure and cell parameters were fitted using Rietveld analysis using the *TOPAS 3.0* software. Scanning Electron Microscopy (SEM) was used in order to study the morphology of the powders using a Leica Cambridge Stereoscan 440 scanning electron microscope fitted with an energy-dispersive X-ray analyzer (EDS). X-ray photoelectron spectroscopy (XPS) was performed using an AES-XPS PHI-548 spectrometer after exciting the samples by an unmonochromatized Al K_α line at 1486.6 eV. The working pressure was $<1 \times 10^{-10}$ Pa. The energy scale was calibrated using thick films of copper with line at 932.67 eV for Cu $2p_{3/2}$. Survey scans were obtained in the 1205-(−10) eV energy interval at 1.0 eV per step, pass energy of 100 eV. Additionally, the high-resolution XPS scans were completed at 0.2 eV energy steps and pass energy of 50 eV (constant pass energy mode). The Electric Impedance Spectroscopy (EIS) measurements were taken in a frequency range from 1 kHz to 1 MHz by means of a Solartron 1260 Impedance Analyzer with a Solartron 1296 Dielectric Interface. Silver paste was applied on the surface of the pellets as electrodes. The temperature was scanned between 298 K and 573 K (25 °C and 300 °C) in steps of 298 K (25 °C), taking a full spectrum with an applied V_{rms} voltage of 1 V for each step. To reach the thermal equilibrium, the temperature of the samples was stabilized for at least 20 minutes before each measurement. Additionally, magnetic measurements were realized with a LDJ-Electronics model 9600 vibrating sample magnetometer with a magnetic field applied of 20 kOe.

III. RESULTS AND DISCUSSION

In this work, the A-site of the $BiFeO_3$ compounds was partially substituted by cations with different ionic radii to cause a distortion in the perovskite structure which could produce improving of the electrical and magnetic properties. Figures 2(a) through (d) display the XRD patterns of the series of compounds with (a) lanthanum (BLFO), (b) yttrium (BYFO), (c) cerium (BCFO), and (d) dysprosium (BDFO) substitution. The major

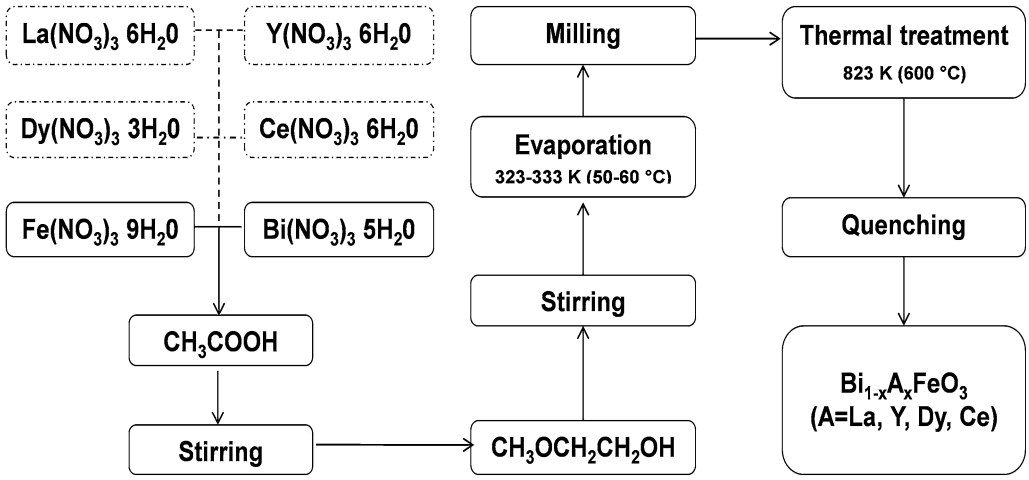

Fig. 1—Experimental setup for sol–gel technique.

diffraction peaks of all the samples match well with the $BiFeO_3$ phase according to the ICDD Card 72-7678; however, some extra peaks were observed at 2θ around 30° which are associated with trace amounts of the mullite-type $Bi_2Fe_4O_9$ and sillenite-type $Bi_{25}FeO_{40}$.[25] The secondary phases are likely formed during the crystallization of the $BiFeO_3$, due to instant changes in the oxygen partial pressure and kinetics of the phase formation.[26,27] The goal of this work was to obtain pure solid solutions of $BiFeO_3$ ceramics and to try to eliminate the undesirable phases; the powders were leached with diluted nitric acid for 5 minutes up to three times, but unfortunately, in some specimens the $BiFeO_3$ phase began to dissolve and the reflections of the impurity phases become stronger. Only, BLFO-0.10 and BLFO-0.15 samples (Figure 2(a)) showed a single phase indicating the formation of solid solutions.

On the other hand, the diverse BLFO samples showed a gradual variation on the diffraction peaks position and diminished their intensity with lanthanum content from 0.05 to 0.20 mol pct. In addition, the reflections (104) and (110) merged to a single peak (Figure 3) suggesting a structural transition[28–31] provoked for the incorporation of the La^{3+} ions into $BiFeO_3$ structure.[31] It is important to mention that some specimens as BYFO-0.10, BDFO-0.05, and BCFO-0.02 samples presented a minimum content of secondary phases compared with other reports.[14,32–36]

X-ray diffraction patterns of the BLFO solid solutions at x = 0.10 and 0.15 were analyzed using Topas Rietveld refinement program (Figure 4). The obtained values of χ^2 ($\chi^2 = R_{wp}/R_{exp}$) (≤1.86) are in a good agreement with those reported in the literature and it can be concluded that a successful refinement was achieved.[28,37,38] Table I shows that the c-axis elongation changes from 13.804 Å to 13.764 Å and diminished the cell volume from 371.76 to 370.56 Å. The structure distortion is attributed to the substitution of Bi^{3+} for La^{3+} in the unit cell[28] and the differences of their ionic radii.[39]

The sintering process is essential to get an adequate grain size and it contributes to reduce dielectric losses driven for holes and grain boundaries in the samples.[40] In this sense, Scanning Electron Microscopy (SEM) was used to determine the grain size and uniformity of the specimens (Figures 5 and 6). Two sintering processes were used on the BLFO-0.10 and BLFO-0.15 solid solutions (Figure 5), spark plasma sintering (SPS) and conventional sintering (CS). SPS is recognized as a novel sintering method of preparing ceramic materials because it uses short sintering periods;[41] however, the pellets

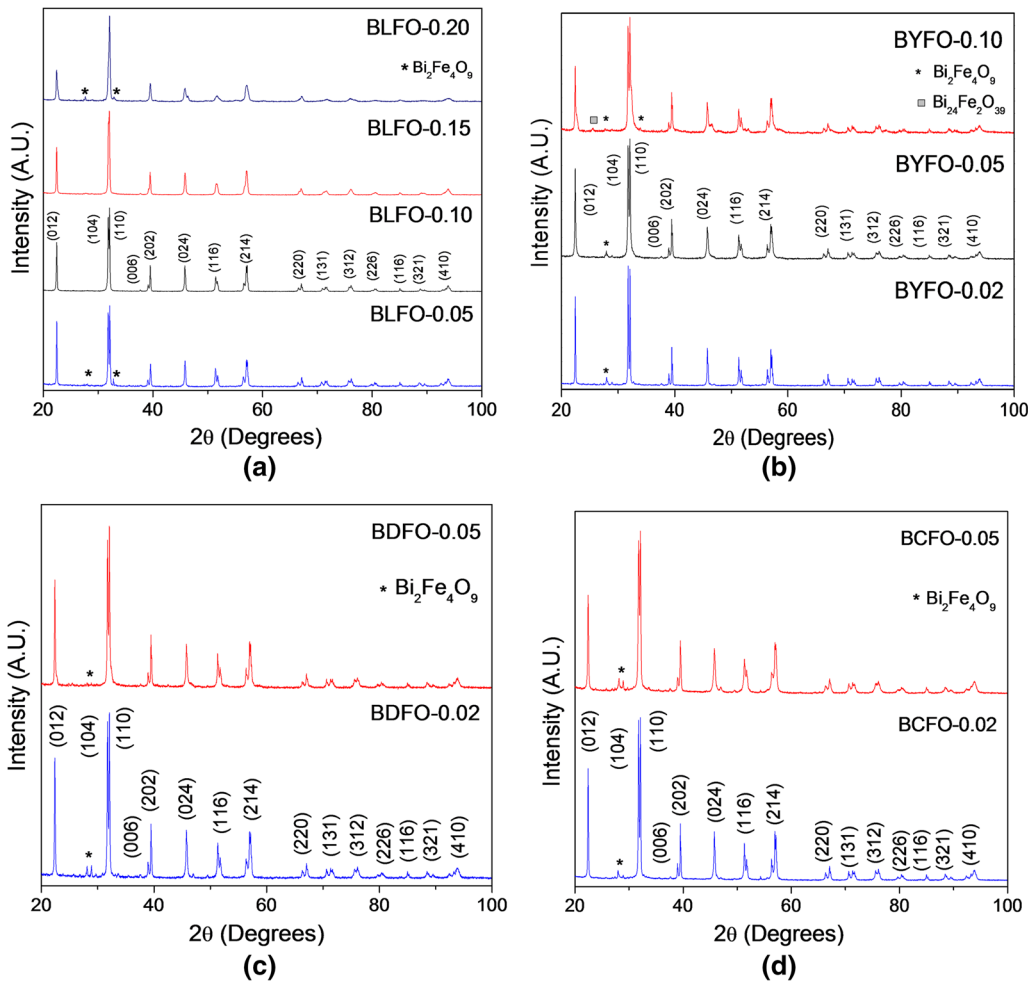

Fig. 2—X-ray data for (*a*) BLFO, (*b*) BYFO, (*c*) BDFO, and (*d*) BCFO powders obtained by the sol–gel method as a function of cation content.

obtained by this technique (Figures 5(a) and (b)) show reduced grain sizes compared with CS pellets (Figures 5(c) and (d)). In addition, SPS pellets shown characteristics grains of secondary phase. Apparently, in these compounds, the fast rate of heat flow avoided the adequate growth of the grains; also, it melted the BFO phase generating evaporation of bismuth (~1103 K (830 °C)) allowing secondary phase formation. On the other hand, the observed grains in the CS pellets are integrated of aggregates of fine-grained crystals which incremented by the low heat flow of the temperature;[42] also, CS pellets (Figures 5(c) and (d)) showed a slight reduction of the grain size according to the increment of dopant content. This difference between lanthanum composition ($x = 0.10$ and 0.15) was observed in other research[43] and it is related to the partial substitution of the bismuth for lanthanum in the $BiFeO_3$ lattice.

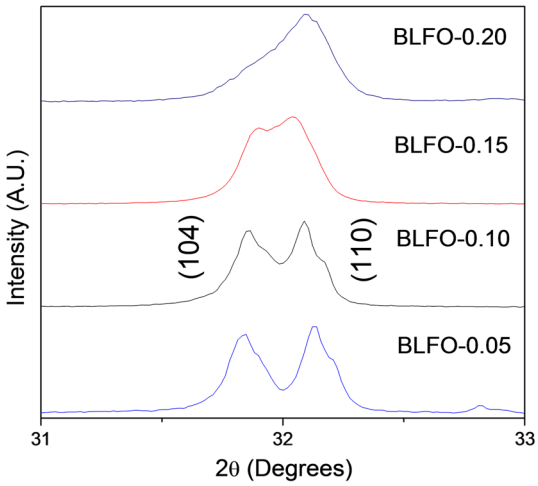

Fig. 3—Enlarged view of the (104) and (110) reflections of the BLFO powders.

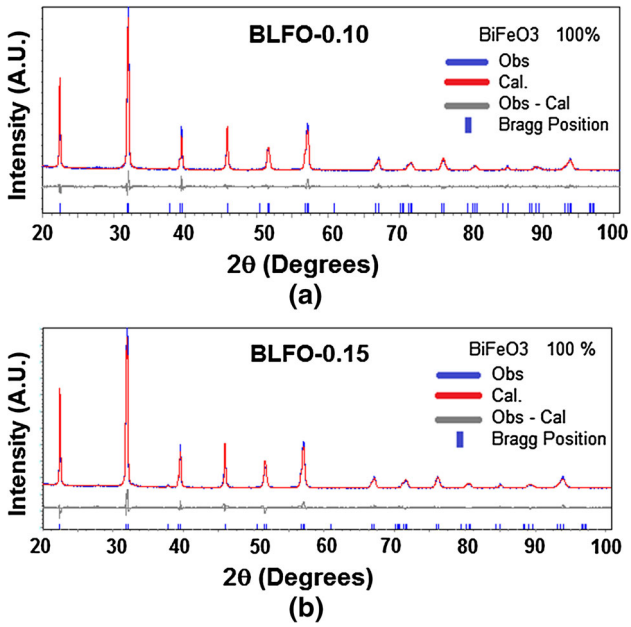

Fig. 4—Rietveld refinement XRD patterns of (*a*) BLFO-0.10 and (*b*) BLFO-0.15 samples.

The specimens with yttrium, dysprosium, and cerium content which presented minor content of secondary phases were sintered by CS (Figure 6). The diverse phases were evidenced by differences in the morphology and it suggests dielectric losses.[40] These results indicate the importance of selecting an adequate sintering process as well as heat flow to maintain a single phase in the samples.

The surface analysis of BLFO-0.10 and BLFO-0.15 solid solutions is presented in Figure 7. The XPS survey spectra revealed the characteristics bismuth and iron peaks of $BiFeO_3$ compounds (Figures 7(a) and (b)). In order to identify the oxygen vacancies, the O 1s XPS spectra were measured (Figures 7(c) and (d)). The BLFO-0.10 specimen presented a broad O 1s peak and it was fitted into three Gaussian curves with peaks in binding energies located at ~530, 531.59, and 533.19 eV. On the other hand, the O 1s peak of BLFO-0.15 specimen presented less Gaussian curves with peaks at ~530 and 532 eV. The lower binding energy represents the oxygen in the lattice,[44,45] while higher binding energies are assigned to absorbed oxygen species, which are related to the presence of oxygen vacancies.[44] These results suggest that oxygen vacancies might have contributions in the dielectric performance.[44,46]

One of the objectives of this work is to enhance the electric performance of the $BiFeO_3$. In this sense, only single-phase compounds (BLFO-0.10 and BLFO-0-15) were characterized by EIS to reduce possible contributions in the dielectric behavior of other phases (Figure 8). The EIS data ($/Z/vs\ f$) were used to obtain the frequency-permittivity plots taking into account the pellet geometric factor and the equations elsewhere reported.[47] The samples displayed a slight increment in the permittivity values compared with other reports;[48,49] however, the BLFO-0.15 specimen (Figure 8(b)) showed a dielectric anomaly at ~ 448 K (175 °C) which provokes diminish its permittivity value. It is important to mention that some dielectric anomalies have been observed close

Table I. Structural Parameters of BLFO-0.10 and BLFO-0.15 Obtained by Rietveld Refinement

				R-Factors (pct)			
Sample	Model	Cell (Å)	Cell Volume	R_{Bragg}	R_p	R_{wp}	χ^2
BLFO-0.10	*R3c*	$a = 5.576$ $c = 13.804$	371.76	1.98	3.76	5.07	1.87
BLFO-0.15	*R3c*	$a = 5.576$ $c = 13.764$	370.56	2.23	3.84	5.09	1.70

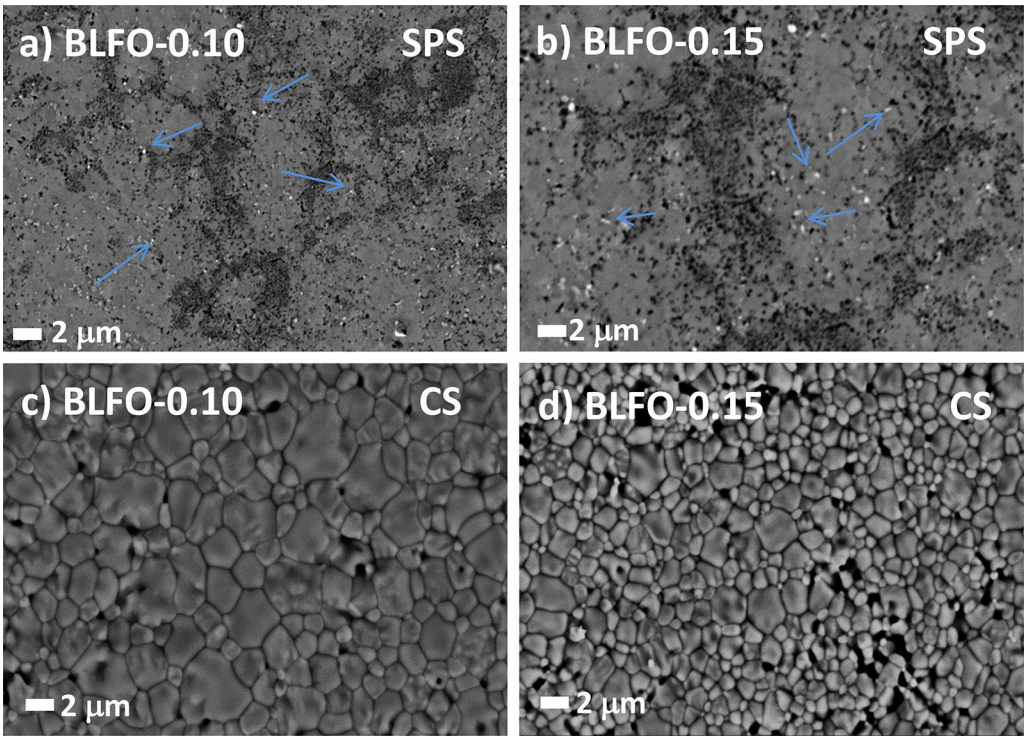

Fig. 5—SEM images of SPS and CS sintering methods of (*a*), (*c*) BLFO-0.10 and (*b*), (*d*) BLFO-0.15 samples.

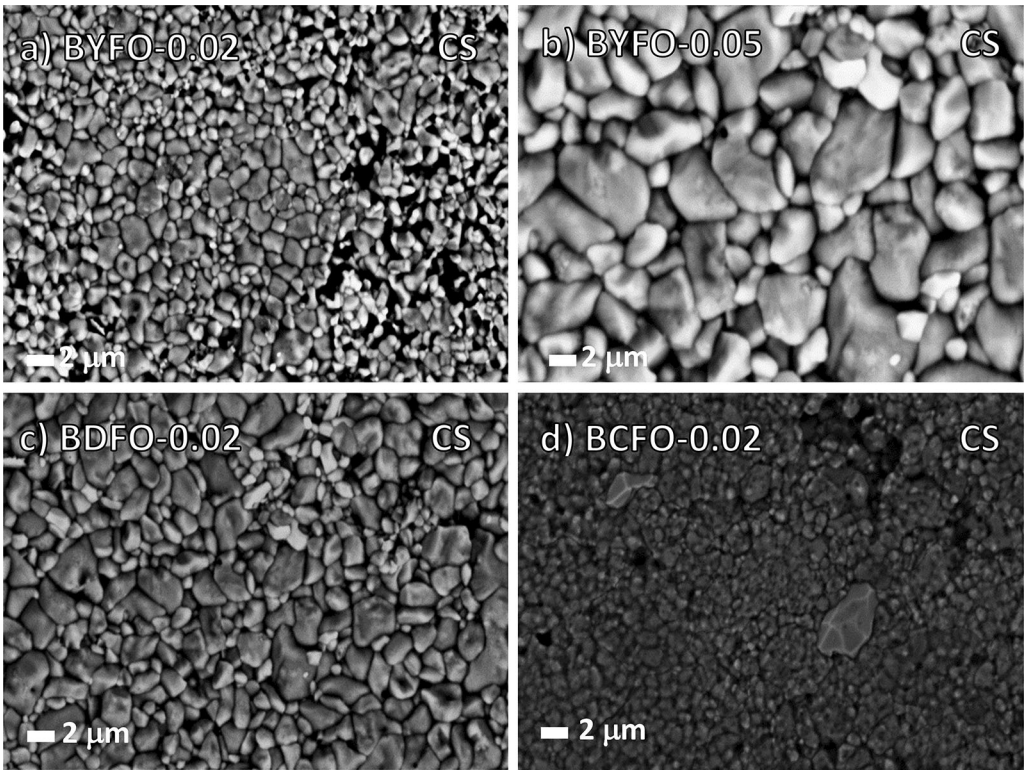

Fig. 6—SEM images of (*a*) BYFO-0.02, (*b*) BYFO-0.05, (*c*) BDFO-0.02, and (*d*) BCFO-0.02 pellets.

to this temperature and they are reported as an artifact caused by the change in the resistivity;[50–53] but, none of them were strong enough.[50] On the other hand, the tan δ values (Figures 8(e) and (f)) indicate high dielectric losses in both specimens confirming the influence of the oxygen vacancies on the electrical response.[44,46]

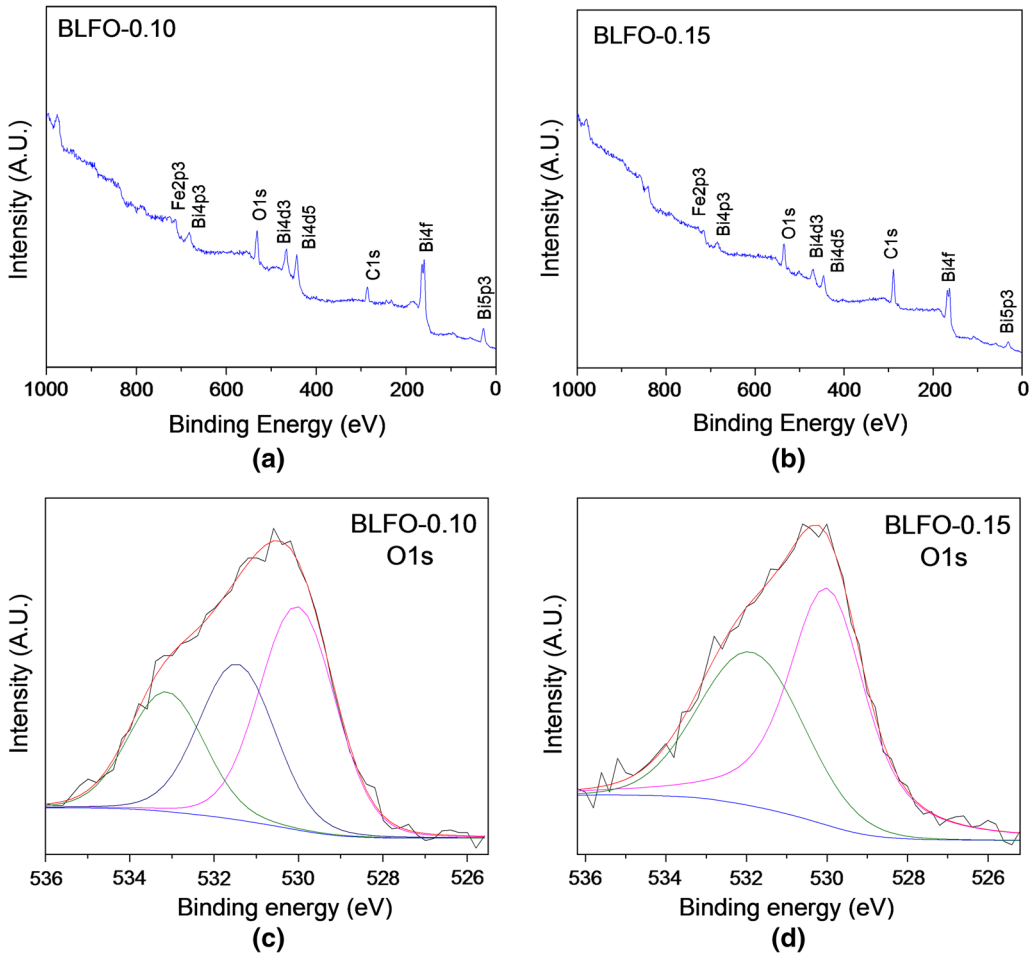

Fig. 7—XPS results of (*a*), (*c*) BLFO-0.10 and (*b*), (*d*) BLFO-0.15 samples.

Probably, other factors could have been contributed in the dielectric anomaly observed in the BLFO-0.15 sample. In this sense, the pellets were analyzed for second time by SEM microscopy (Figure 9) to examine some possible contributions caused for a hide secondary phase. An inside view of the BLFO-0.10 and BLFO-0.15 pellets (Figures 9(a) through (c)) confirms that only a single phase is present and no evidence of secondary phases was detected, although more grain boundaries were detected in the BLFO-0.15 specimen and it provokes dielectric losses. After EIS measurements (Figures 9(b) through (d)), several changes in the grains were observed. The grains presented considerable holes caused for the EIS measurements being more pronounced in the BLFO-0.15 specimen (Figure 9(d)) and possibly it contributed to the dielectric anomaly; however, more studies need to be realized.

It is known that $BiFeO_3$ has partially filled 3d orbits of the *B*-site Fe^{3+} ion which causes *G*-type canted antiferromagnetic order as well as an incommensurate space-modulated spin structure. Nonetheless, the presence of such a space-modulated spin structure cancels out the possible non-zero remnant magnetization allowed by the canting angle of *G*-type canted antiferromagnetic order leading to null macroscopic magnetization.[39,54] The magnetic hysteresis loops at room temperature for BLFO ($x = 0.05$ to 0.20), BYFO-0.02, and BDFO-0.05 are shown in Figure 10. The La^{3+} substitution provoked a weak ferromagnetism in the BLFO-0.05 sample with a magnetization value of ~0.03 emu/g and a coercivity of ~130 Oe (Fi. 8a);[8,55,56] in spite of that, a significant enhancement was observed with the increment of the dopant up to ~0.3 emu/g and ~7782 Oe (Figures 10(b) through (d)).[40] It is known that a possible enhancement in the magnetic properties could be caused by the presence of small magnetic impurities,[39] but no impurities were detected in the BLFO-0.10 and BLFO-0.15 samples and the coercivity tendency continues with the dopant increment. In this sense, this enhancement in the magnetization could be attributed to the modification in the lattice caused by the Lanthanum substitution, in agreement with other researches.[39,57,58] On the other hand, the compounds with yttrium and dysprosium addition (Figures 10(e) and (f)) showed similar hysteresis effects than lanthanum showing weak ferromagnetism, even though these samples were polycrystalline compounds.

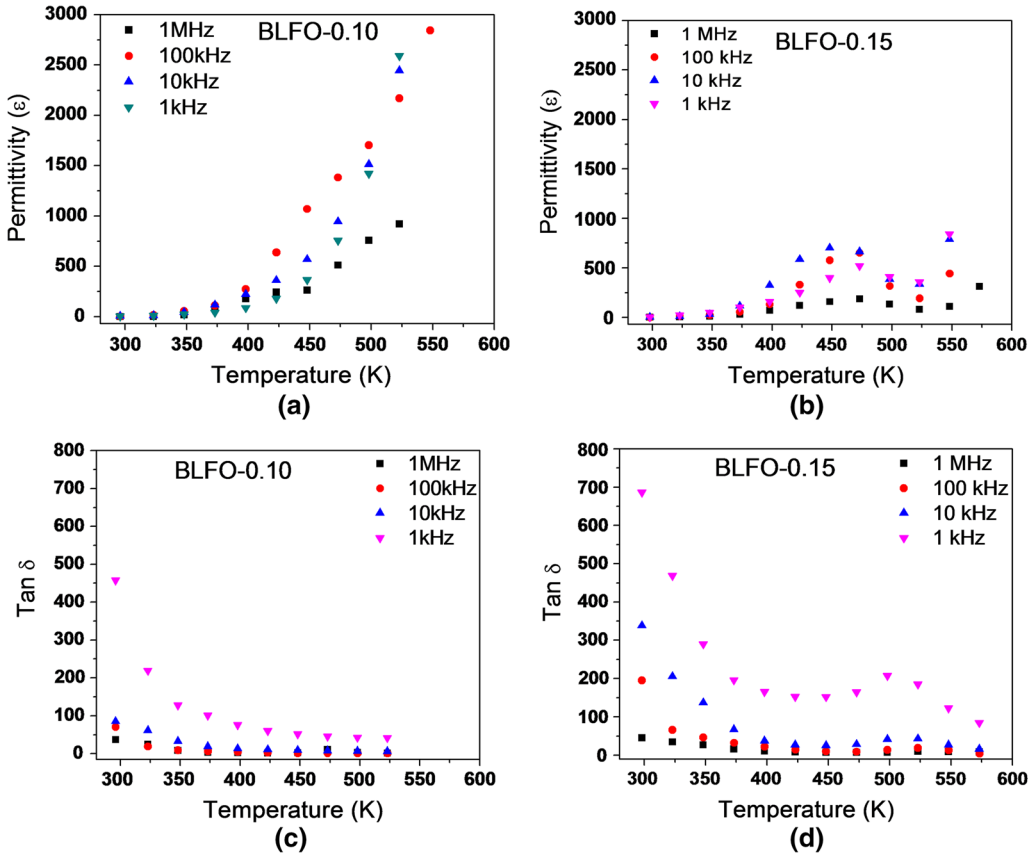

Fig. 8—Permittivity (ε') and tan δ of: (*a*), (*c*) BLFO-0.10 and (*b*), (*d*) BLFO-0.15 samples.

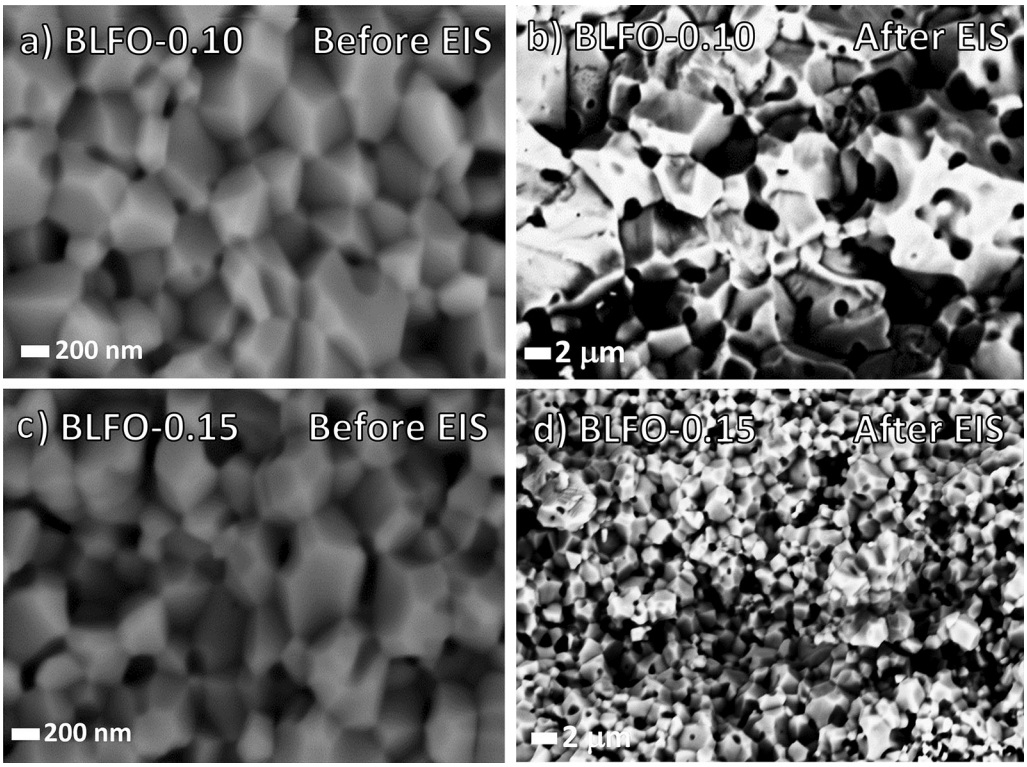

Fig. 9—SEM images before and after of EIS measurements of (*a*), (*b*) BLFO-0.10 and (*c*), (*d*) BLFO-0.15 samples.

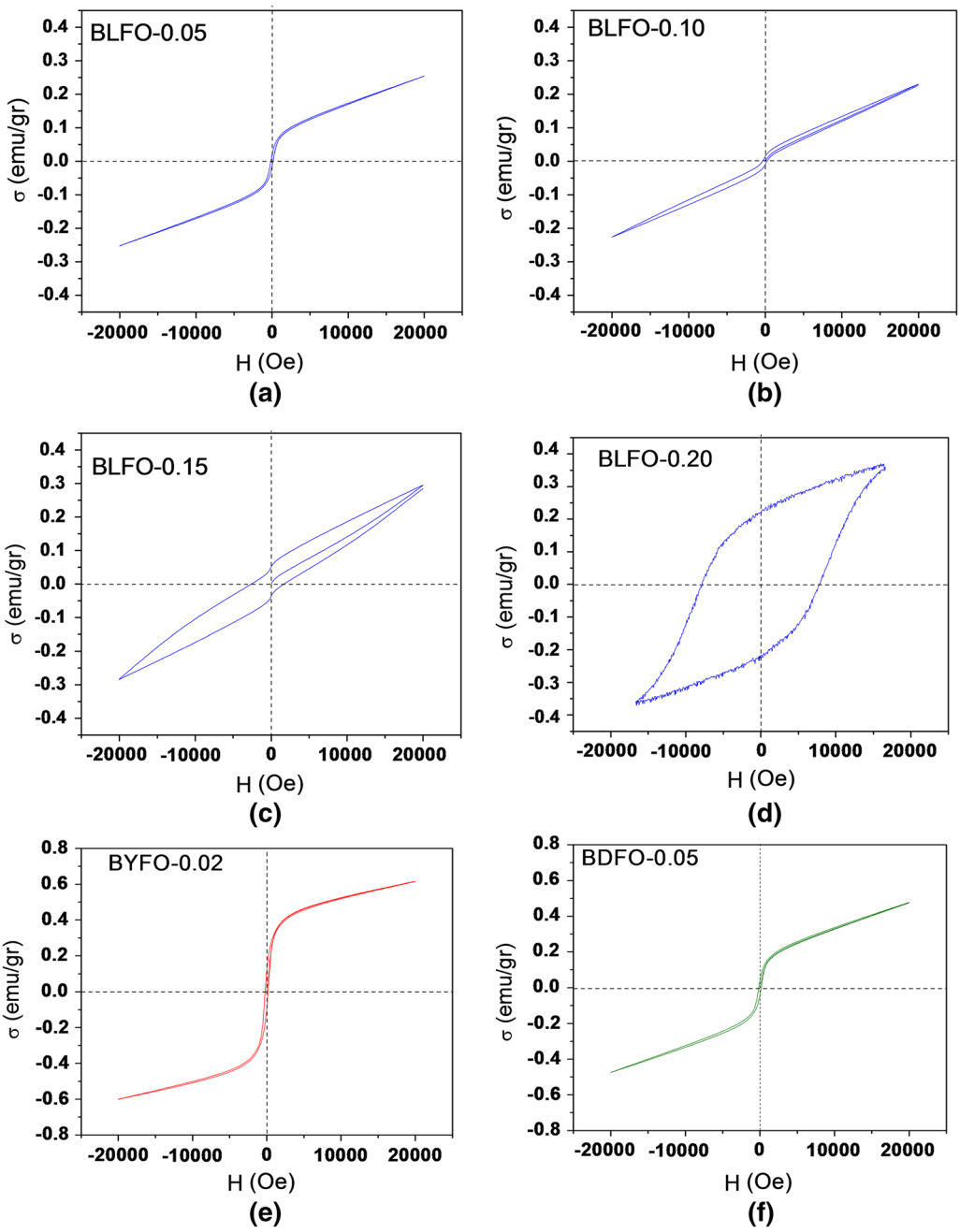

Fig. 10—Magnetic hysteresis loops of (*a*) BLFO-0.05, (*b*) BLFO-0.10, (*c*) BLFO-0.15, (*d*) BLFO-0.20, (*e*) BYFO-0.02, and (*f*) BDFO-0.05 measured at room temperature.

IV. CONCLUSIONS

In this work, it has been demonstrated that it is possible to reach a single phase during the preparation of RE cations doping on multiferroic $BiFeO_3$ compounds by proper modulation of synthesis parameters. XRD and Rietveld refinement measurements indicate that under the evaluated conditions and using an atomic percent of 0.10 and 0.15, a pure phase was obtained using the lanthanum cation. EIS measurements presented a slight increment in the permittivity values; however, a dielectric anomaly was also observed suggesting that is necessary to optimize the sintering process to get a better performance in these materials (Figures 9 and 10). Finally, the magnetic measurements revealed an enhancement on the coercive field in the BLFO compounds due to the lattice modification during the doping process and it depends on lanthanum amount. The results of these studies are very promising and suggested that BLFO compounds with 0.10 and 0.15 of lanthanum can be attractive for use as storage element in non-volatile ferroelectric and magnetic random access memories.

ACKNOWLEDGMENTS

David S. García Zaleta is grateful for his postgraduate fellowship to SIP-IPN and COFAA-IPN. The authors are also grateful for the financial support provided by CONACYT through the CB2009-132660 and CB2009-133618 Projects and to IPN through SIP 2015-0202 and 2015-0227 Projects and SNI-CONACYT. Authors wish to thank for the technical support during magnetic measurements of IIM-UNAM.

REFERENCES

1. V. Antanov, I. Georgieva, N. Trendafilova, and D. Kovacheva: *Solid State Sci.*, 2012, vol. 14, pp. 782–88.
2. S. Karimi, I.M. Reaney, I. Levin, and I. Sterianou: *Appl. Phys. Lett.*, 2009, vol. 94, p. 112903.
3. F. Kubel and H. Schmid: *Acta Crystallogr. Sect. B*, 1990, vol. 46, p. 698.
4. Ye. Roginska, Yy. Tomashpo, Yn. Venevtse, V.M. Petrov, and G.S. Zhdamov: *Soviet Physics JETP-USSR.*, 1966, vol. 23, p. 47.
5. Z. Yu-jie, Z. Hong-guo, Y. Jin-hua, and Z. Hong-wei: *J. Magn. Magn. Mater.*, 2010, vol. 322, pp. 2251–55.
6. K. Sang-Su and K. Won-Jeong: *Mater. Lett.*, 2005, vol. 59, pp. 4006–09.
7. Z.X. Cheng, A.H. Li, and X.I. Wang: *J. Appl. Phys.*, 2008, vol. 103, pp. 878–81.
8. D. Maurya, H. Thota, K.S. Nalwa, and A. Garg: *J. Alloys Compd.*, 2009, vol. 477, pp. 780–84.
9. J. Prado-Gonjal, M.E. Villafuerte-Castrejón, L. Fuentes, and E. Morán: *Mater. Res. Bull.*, 2009, vol. 44, pp. 1734–37.
10. M.B. Bellakki, V. Manivannan, and C. Madhu: *Mater. Chem. Phys.*, 2009, vol. 116, pp. 599–602.
11. P. Fischer, M. Polomska, and I. Sosnowska: *J. Phys. C: Solid State Phys.*, 1980, vol. 13, pp. 1931–40.
12. E.I. Speranskaya, V.M. Skorikov, E.Ya. Kode, and V.A. Terectova: *Bull. Acad. Sci.*, 1965, vol. 5, pp. 873–74.
13. A. Maitre, M. Francois, and J.C. Gachon: *J. Phase Equilib. Diffus.*, 2004, vol. 25, pp. 59–67.
14. J. Xu, G. Ye, and M. Zeng: *J. Alloys Compd.*, 2014, vol. 587, pp. 308–12.
15. G. Dong, G. Tan, W. Liu, A. Xia, and H. Ren: *Ceram. Int.*, 2014, vol. 40, pp. 919–1925.
16. X. Yan, J. Chen, and U. Qi: *J. Eur. Ceram. Soc.*, 2010, vol. 30, pp. 265–69.
17. R. Xiao, V.O. Pelenovich, and D. Fu: *Appl. Phys. Lett.*, 2013, vol. 103, pp. 012901–04.
18. S.K. Pradhan and B.K. Roul: *Phys. B*, 2012, vol. 407, pp. 2527–32.
19. G.S. Lotey and N.K. Verma: *Superlattices Microstruct.*, 2013, vol. 53, pp. 184–94.
20. Y. Lin, Q. Jiang, Y. Wang, and C.W. Nan: *Appl. Phys. Lett.*, 2007, vol. 90, p. 172507.
21. I. Levion, M.G. Tucker, H. Wu, V. Provenzano, C.L. Dennis, and S. Karimi: *Chem. Mater.*, 2011, vol. 23, pp. 2166–75.
22. I. Sosnowska, T. Pterlin-Neumaier, and E. Steichele: *J. Phys. C.*, 1982, vol. 15, p. 4835.
23. G.L. Yuan, S.W. Or, J.M. Liu, and Z.G. Liu: *Appl. Phys. Lett.*, 2006, vol. 89, pp. 052905–07.
24. V.A. Khomchenko, V.V. Shvartsman, P. Borisov, and W. Kleemann: *Acta Mater.*, 2009, vol. 57, pp. 5137–45.
25. V. Koval, I. Skorvanek, M. Reece, L. Mitoseriu, and H. Yan: *J. Eur. Ceram. Soc.*, 2014, vol. 34, pp. 641–51.
26. G.D. Achenbach, W.J. James, and R. Gerson: *J. Am. Ceram. Soc.*, 1967, vol. 50, p. 437.
27. M.S. Bernardo, T. Jardiel, M. Peiteato, A.-C.- Caballero, and M. Villegas: *J. Eur. Ceram. Soc.*, 2011, vol. 31, pp. 3047–53.
28. A.Z. Simões and F. Gonzalez-Garcia: *Mater. Chem. Phys.*, 2009, vol. 116, pp. 305–09.
29. F. Gonzalez-Garcia, C.S. Riccardi, and A.Z. Simões: *J. Alloys Compd.*, 2010, vol. 501, pp. 25–29.
30. X. Li, X. Wang, Y. Li, W. Mao, and P. Li: *Mater. Lett.*, 2013, vol. 90, pp. 152–55.
31. X. Yan, J. Chen, Y. Qi, J. Cheng, and Z. Meng: *J. Eur. Ceram. Soc.*, 2010, vol. 30, pp. 265–69.
32. K. Koval, I. Skorvanek, M. Reece, L. Mitoseriu, and H. Yan: *J. Eur. Ceram. Soc.*, 2014, vol. 34, pp. 641–51.
33. S. Zhang, W. Luo, D. Wang, and Y. Ma: *Mater. Lett.*, 2009, vol. 63, pp. 1820–22.
34. J. Xu, G. Wang, H. Wang, D. Ding, and Y. He: *Mater. Lett.*, 2009, vol. 63, pp. 855–57.
35. L. Luo, W. Wei, X. Yuan, K. Shen, M. Xu, and Q. Xu: *J. Alloy Compd.*, 2012, vol. 540, pp. 36–38.
36. J. Liu, M. Li, L. Pei, J. Wang, B. Yu, X. Wang, and X. Zhao: *J. Alloys Compd.*, 2010, vol. 493, pp. 544–48.
37. A. Sagdeo, P. Mondal, A. Upadhyay, A.K. Sinha, A.K. Srivastava, S.M. Gupta, P. Chowdhury, T. Ganguli, and S.K. Deb: *Solid State Sci.*, 2013, vol. 18, pp. 1–9.
38. A. Srivastava, H.K. Singh, V.P.S. Awana, and O.N. Srivastava: *J. Alloys Compd.*, 2013, vol. 552, pp. 336–44.
39. P. Suresh and S. Srinath: *J. Alloy. Compds.*, 2013, vol. 554, pp. 271–76.
40. M.E. Lines and A.M. Glass: *Principles and Applications of Ferroelectrics and Related Materials*, Clarendon Press, Oxford, 1977, pp. 531–545.
41. S.-H. Song, Q.-S. Zhu, L.-Q. Weng, and V.R. Mudinepalli: *J. Eur. Ceram. Soc.*, 2015, vol. 35, pp. 131–38.
42. WD Kingery: *Introduction to Ceramics*, Wiley, New York, 1960.
43. D.S. Garcia-Zaleta, A.M. Torres-Huerta, M.A. Dominguez-Crespo, J.A. Matutes-Aquino, A.M. Gonzalez, and M.E. Villafuerte-Castrejón: *Ceram. Int.*, 2014, vol. 40, pp. 9225–33.
44. K. Min, F. Huang, Y. Jin, W. Zhu, and J. Zhu: *Ferroelectrics*, 2013, vol. 450, pp. 42–48.
45. T. Gao, Z. Chen, Y. Zhu, F. Niu, Q. Huang, L. Qin, X. Sun, and Y. Huang: *Mater. Res. Bull.*, 2014, vol. 59, pp. 6–12.
46. G.L. Yuan, K.Z. Baba-Kishi, J.-M. Liu, and S. Wing-Or: *J. Am. Ceram. Soc.*, 2006, vol. 89, pp. 3136–39.
47. ME Lines and AM Glass: *Principles and applications of ferroelectrics and related materials*, Clarendon Press, Oxford, 1977, pp. 531–545.
48. Y.H. Lee, J.M. Wu, and C.H. Lai: *Appl. Phys. Lett.*, 2006, vol. 88, p. 042903.
49. G.L. Yuan, S.W. Or, Y.P. Wang, Z.G. Liu, and J.M. Liu: *Solid State Commun.*, 2006, vol. 138, pp. 76–81.
50. G. Catalan and J.F. Scott: *Adv. Mater.*, 2009, vol. 21, pp. 2463–85.
51. R. Mazumder, S. Ghosh, P. Mondal, D. Bachattacharya, S. Dasgupta, N. Das, A. Sen, A.K. Tyagi, M. Sivakimar, T. Takami, and H. Ikuta: *J. Appl. Phys.*, 2006, vol. 100, p. 033908.
52. G. Catalan: *Appl. Phys. Lett.*, 2006, vol. 88, p. 102902.
53. G. Catalan and J.F. Scott: *Nature*, 2007, vol. 448, pp. E4–E5.
54. G.L. Yuan, S.W. Or, and H.L.W. Chan: *J. Phys. D Appl. Phys.*, 2007, vol. 40, pp. 1196–1200.
55. S Kazhugasalamoorthy, P Jegatheesan, R Mohandoss, NV Giridharan, B Karthikeyan, RJ Joseyphus, and S Dhanuskodi: *J. Alloy Compd.*, 2010, vol. 493, pp. 569–72.
56. X. Zheng, Q. Xu, Z. Wen, X. Lang, D. Wu, T. Qiu, and M.X. Xu: *J. Alloy Compd.*, 2010, vol. 499, pp. 108–12.
57. V.A. Khomchenko, D.A. Kiselev, J.M. Vieira, L. Jian, and A.L. Kholkin: *J. Appl. Phys.*, 2008, vol. 103, pp. 024105–06.
58. R. Rai, S.K. Mishra, N.K. Singh, S. Sherma, and A.L. Kholkin: *Curr. Appl. Phys.*, 2011, vol. 11, pp. 508–12.